Interaction between plastic deformation and hydrogen damage behavior of 30CrMnSiNi2A steel

Lei Fu, Hongyuan Fang

State Key Laboratory of Advanced Welding and Joining, Harbin Institute of Technology, Harbin,150001, China

Abstract. The interaction between plastic deformation and hydrogen damage behavior of 30CrMnSiNi2A steel was investigated by pre-strain tensile tests and hydrogen charging by electrochemical method. This paper mainly contains two parts. The plastic deformation was restrained by hydrogen-charged, and the effect of hydrogen brittleness damage behavior was accelerated by pre-plastic deformation measure. Tensile pre-strian tests with hydrogen charging at current density from 0 to 50 mA/cm^2 for 120 min were performed at room temperature. Both rate of reduction in area and elongation were decreased due to the transition from ductile to brittle fracture by hydrogen charging, which meant the ability of plastic deformation was reduced by hydrogen. With hydrogen concentration increasing, yield strength also increased indicating that the plastic deformation forming conditions of steel were improved by hydrogen. Hydrogen content increased with pre-strain measured by glycerol gas collection method. Due to the pre-strain measure before hydrogen charging, the reduction of area and elongation were further reduced, while the strength was unexpectedly low. It was because pre-strain promoted the formation of hydrogen-induced crackings (HIC). This proved that the plastic deformation promoted the generation of hydrogen damage.

1 Introduction

The problem of hydrogen embrittlement in industrial applications has attracted enormous attention for years, which is particularly severe in the high-strength steels. Hydrogen embrittlement attributes to the degradation of mechanical properties of mild steel after corrosion [1]. Blades of the Maraging steel is sensitive to hydrogen embrittlement phenomenon proved by experiments [2]. The chemical composition of high-Mn steels and hydrogen embrittlement sensitivity are closely related as the material's stacking fault energy and phase stability were also affected simultaneously [3]. When the martensitic advanced high-strength steel is in low pH in 3.5% NaCl, hydrogen embrittlement susceptibility increased with increasingly negative potentials [4]. For achieving high resistance to hydrogen embrittlement, the high carbon manganese steel can be introduced nano-twins microstructures [5]. The addition of Ti content in hot-stamped boron steels is another method that can be used to enhance the resistance to hydrogen embrittlement [6]. Refining microstructure of quenched-partitioned-tempered low carbon steel also improves the hydrogen embrittlement resistance [7].

Susceptibility to hydrogen embrittlement changes with materials that have been mechanically treated. Hydrogen embrittlement sensitivity was decreased after laser peening due to the basis of compressive residual stress and dislocation changes [8]. Some documents also reported that pre-strain can also affect the hydrogen embrittlement sensitivity [9-11]. Pre-strain increased the resistance to hydrogen embrittlement in STS 310S by suppressing the transition of a ductile to brittle fracture [9]. As the pre-strain increases, the hydrogen embrittlement sensitivity of screw-thread steel bars increases first and then decreases [10]. However, pre-strain does not show sufficient effect on hydrogen embrittlement susceptibility of high-entropy alloy [11].

30CrMnSiNi2A is a kind of low-alloyed martensite ultra-high strength steel with remarkable application in many industries which is sensitive to stress corrosion cracking [12] and hydrogen embrittlement [13]. With respect to the 30CriMnSiNi2A steel, the effect of pre-strain on hydrogen embrittlement has rarely been investigated. Therefore, it is necessary to study the effect of pre-strain on hydrogen embrittlement of 30CriMnSiNi2A steel. This paper also helps explain the mechanism of hydrogen embrittlement for 30CriMnSiNi2A steel from the perspective of macroscopic experiments and microscopic fracture.

2 Experimental

2.1 Materials and samples

The tested steel used in this investigation, 30CrMnSiNi2, was a kind of low alloy ultra-high strength steel with the chemical composition listed in table 1.

Hot-rolled rods of 30 mm in diameter and 70 mm in length were austenitised at 890 ℃ for 25 min and then cooling slowly in the air. The test samples were taken along the hot-rolled rods longitudinal direction; their shape and dimension being illustrated in figure 1.

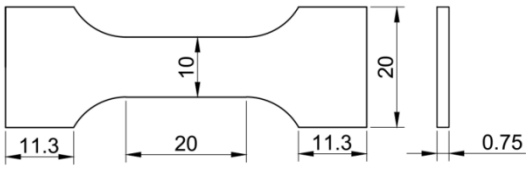

Figure 1. Dimension of tensile sample (mm).

2.2 Pre-strain test

Sample A was stretched to rupture directly in order to observe the origin mechanical properties and fracture morphology. The tensile elongation (failure strain) of the uncharged sample was 13.7% (as shown in figure 2). Samples (C2 and D2) were stretched to the engineering strain of 6.6% and 4.8% respectively (i.e. pre-stain) and uniform deformation was observed without necking obviously. Pre-strain tests were performed at rates of 2.8×10^{-3} s^{-1} by the tensile testing machine at room temperature.

Table 1. Chemical composition of high-strength steel (wt %)

C	Mn	Si	Cr	Ni	S	P	Fe
0.30	1.1	1.05	1.05	1.6	0.010	0.015	Bal

2.3 Electrochemical hydrogen charging and measuring test

In order to fill the samples with hydrogen atoms, electrolytic hydrogen charging method was utilized, which set the sample as the cathode, a platinum electrode as the anode, a constant current source as the power supply and the acid solution as the electrolyte. The acid solution of 0.5 mol/L H_2SO_4 was added 0.5 g/L $NaAsO_2$ as the toxic agent to promote a greater proportion of hydrogen atoms produced from cathode into the sample [14].

Sample B, C1 and D1 were charged with hydrogen at the current density of 5, 30 and 50 mA/cm^2 respectively for 10, 2 and 2 hours to observe the effect of hydrogen embrittlement. The sample B was charged hydrogen with current density of 5 mA/cm^2 for 10 hours to prove that small hydrogen charging current density had no significant effect even for long duration. The hydrogen charging parameters of time and current density were presented in table 2.

Hydrogen concentration in samples was measured by glycerol gas collection method in a water bath at 40 ℃ for 72 hours. Samples were measured under the same strain and hydrogen charging conditions as said before. The volume of diffusible hydrogen was measured and then converted to the concentration unit needed, as seen in figure 3.

It can be seen from figure 3 that as the hydrogen charging current density increases, the diffusion hydrogen content also increases. However, the hydrogen concentration of the sample after pre-strain treatment is significantly higher than the hydrogen concentration without pres-train. Several documents also reported that the content of hydrogen increased with pre-strain [10,15,16]. For screw-thread steel bars, the amount of hydrogen increases linearly with the exponent of pre-strain [10]. When a medium-carbon steel is preloaded, the quantity of hydrogen increases proved by thermal desorption test around 50 ℃ to 200 ℃ [15]. The reason for the increase in hydrogen quantity is that the pre-strain increases the number of hydrogen trap sites verified by heat-treated transformation induced plasticity steel [16].

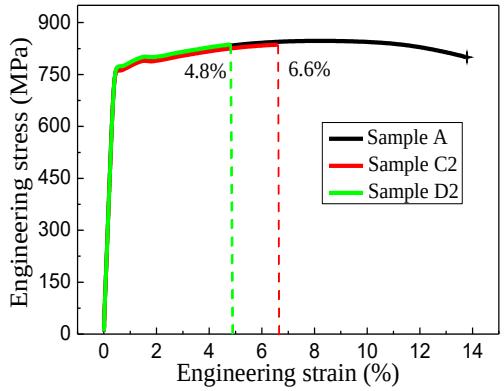

Figure 2. Engineering stress-strain curves.

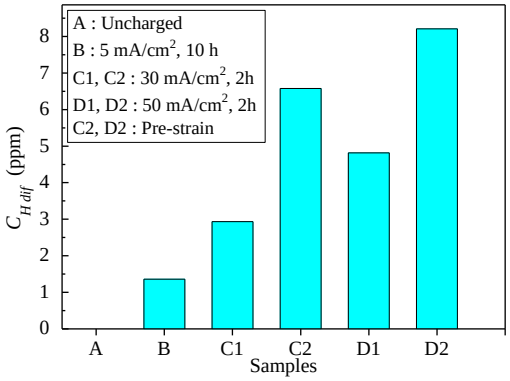

Figure 3. Diffusion hydrogen concentration.

2.4 Tensile test

Engineering stress-engineering strain curves are obtained after hydrogen charging and tensile tests, as seen in figure 4(a). Data of the rates of reduction in area (*Z*) is also displayed in figure 4(b). Results of the tensile tests performed on the samples with and without pre-strain before and after hydrogen (H) charging are displayed in table 2, from which the following three observations can be made.

Firstly, H charging does affect the ductility of 30CrMnSiNi2A steel in significant manner. Hydrogen charging causes the samples to become brittle, reduce the

reduction in area and decrease the elongation, that is, hydrogen reduces the plastic deformability. With the increase in the quantity of hydrogen, this change becomes more pronounced. Secondly, pre-strain accelerates hydrogen embrittlement, leading to a sharp drop in fracture strength. This may be due to the increase in hydrogen trap sites caused by plastic strain [16]. Finally, in samples without pre-strian, H charging leads to an increase in the yield strength (σ_s), that is, the conditions for the onset of plastic deformation increase. Several documents also reported that the quantity of hydrogen increased the yield strength. The yield stress of austenitic stainless steel increases substantially with the increase in hydrogen charging time [17, 18].

Table 2. Conditions of hydrogen charging and pre-stain data

	H-charged		Pre-strain		Total		C_H (ppm)	σ_s (MPa)
	I/S (mA/cm^2)	t (h)	Z (%)	ε (%)	Z (%)	ε (%)		
A	0	0	0	0	10.0	13.7	0	767
B	5	10	0	0	9.2	10.8	1.36	802
C1	30	2	0	0	7.2	7.1	2.93	831
C2	30	2	4.6	6.6	4.8	6.9	6.58	--
D1	50	2	0	0	5.1	5.2	4.82	887
D2	50	2	3.4	4.8	3.5	5.2	8.21	--

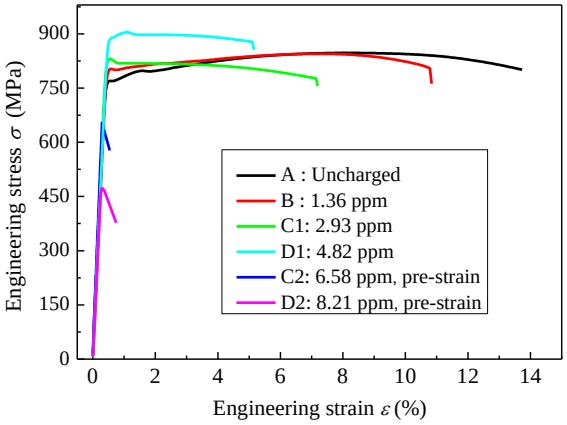

(a) Engineering stress-engineering strain curves

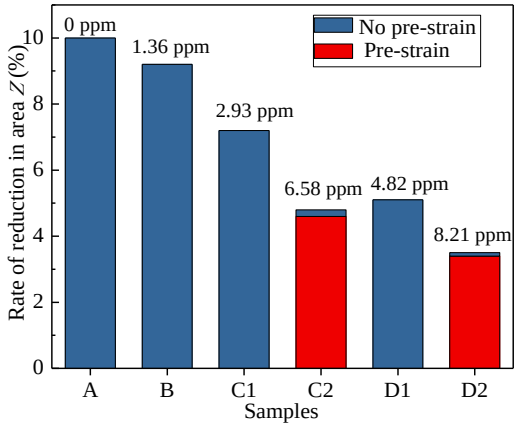

(b) Data of the rates of reduction in area

Figure 4. Change in mechanical properties after hydrogen charging.

3 Result analysis

3.1 Fracture morphology

The fracture surfaces of hydrogen free and hydrogen charged 30CrMnSiNi2A steel samples without and with pre-strain after tensile tests are displayed in figure 5 and figure 6, respectively. The low magnification image of fracture surface of the hydrogen free sample exhibits ductile fracture with apparent necking feature, as demonstrated in figure 5(a). The fracture surface consists of two regions, i.e., central crack initiation which is normal to tensile stress and propagation region (shear lip region) typically at 45° slope to the tensile stress direction which is the maximum shear stress direction. The high magnification image at the shear lip region show dimple fracture with a range of dimple sizes, as shown in figure 5(b).

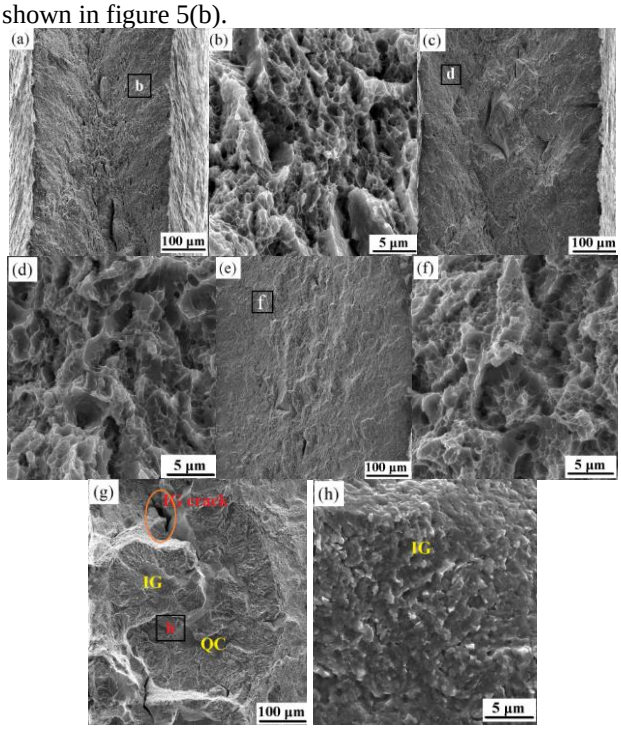

Figure 5. SEM micrograph of hydrogen free and hydrogen charged 30CrMnSiNi2A steel samples without pre-strain (a) overview of fracture surface of sample A without H; (b) high magnification image of the signified region in image(a); (c) overview of fracture surface of sample B with H of 1.36 ppm; (d) high magnification image of the signified region in image(c); (e) overview of fracture surface of sample C1 with H of 2.93 ppm; (f) high magnification image of the signified region in image(e); (g) overview of fracture surface of sample D1 with H

of 4.82 ppm; (h) high magnification image of the signified region in image(g). QC: quasi-cleavage; IG: intergranular fracture.

In the presence of hydrogen (1.36 ppm and 2.93 ppm), the fracture surfaces of sample B and C1 remain ductile with dimple fracture mode, as indicated by figures 5(d) and 5(f) respectively. However, the proportion of the shear lip region in the entire cross section decreases as the hydrogen concentration increases, as seen in figures 5(c) and 5(e), which corresponds to a reduction in the rate of reduction of the area due to hydrogen charged, as shown in figure 4(b). For sample D1 with H of 4.82 ppm, brittle fracture surface with a mixed fracture mode of intergranular fracture (IG) and quasi-cleavage fracture (QC) is observed, as illustrated in figures 5(g) and 5(h). This result shows that when the hydrogen quantity reaches a certain value, the 30CrMnSiNi2A steel undergoes a ductile-brittle transition, and the plastic deformability is further reduced.

For the samples with pre-strain, the fracture surfaces are divided into two diametrically opposed regions, as illustrated in figures 6(a) and 6(d). A part of the fracture surface has covered with IG and QC fracture (figures 6(b) and 6(e)), and fine microvoid coalescence fracture (MVC) occupies other area (figures 6(c) and 6(f)). Since the fracture strength of the pre-strained samples is significantly lower than the yield strength, there may be already hydrogen damage (hydrogen bubbling or hydrogen induced cracking) in the samples before the tensile test. The IG and QC fracture zone is featured by several semi-ellipsoidal pits, as shown in figures 6(a) and 6(d), which may be the hydrogen damage due to the sufficient hydrogen charged.

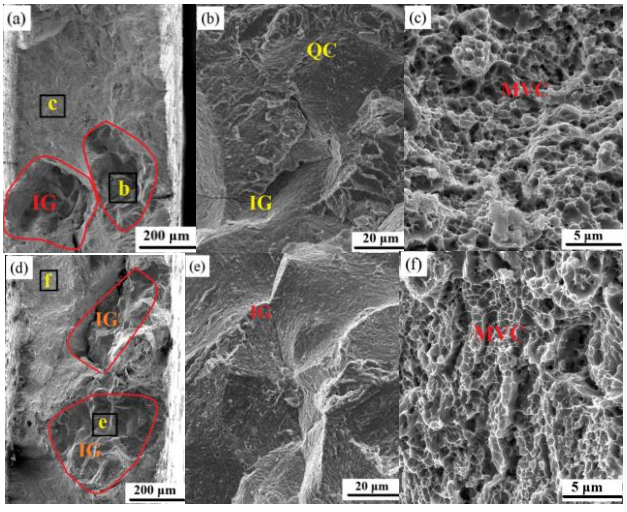

Figure 6. Microstructure of 30CrMnSiNi2A steel samples with pre-strain (a) overview of fracture surface of sample C2 with H of 6.58 ppm; (b) high magnification image of the signified region in image(a); (c) high magnification image of the signified region in image(a); (d) overview of fracture surface of sample D2 with H of 8.21 ppm; (e) high magnification image of the signified region in image(d); (f) high magnification image of the signified region in image(d). QC: quasi-cleavage; IG: intergranular fracture; MVC: micro-void coalescence.

3.2 Metallographic photos

Figure 7 shows the hydrogen-induced cracking (HIC) of the 30CrMnSiNi2A steel samples with pre-stain before tensile tests including transverse and longitudinal cracks. As hydrogen concentration increases, the number of cracks increases. The presence of cracks in the specimen leads to crack growth at low stress. This explains why the fracture strengths of pre-strained samples are lower than yield strengths. This result shows that the reason that the plastic deformation promotes hydrogen damage is to accelerate the generation of hydrogen-induced crackings.

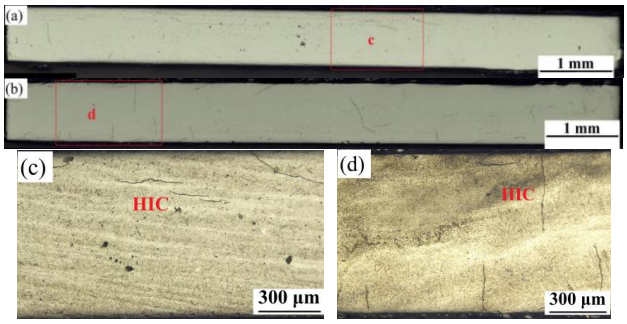

Figure 7. OM views of 30CrMnSiNi2A steel samples with pre-strain after hydrogen charging (a) overview of sample C2 with H of 6.58 ppm; (b) overview of fracture surface of sample D2 with H of 8.21 ppm; (c) high magnification image of the signified region in image(a); (d) high magnification image of the signified region in image(b). HIC: hydrogen-induced cracking.

4 Conclusion

To summarize, the interaction of plastic deformation and the hydrogen damage of 30CrMnSiNi2A steel was investigated, results of which show that the plastic deformation of 30CrMnSiNi2A steel is suppressed and hydrogen embrittlement is accelerated by pre-strains. This is because pre-straining does enhance the H solubility in the steel and then promote hydrogen induced cracking.

References

1. Li L, Mahmoodian M, Li CQ and Robert D 2018 *Constr. Build. Mater.* **170** 78–90
2. Barsanti M, Beghini M, Frasconi F, Ishak R, Monelli B D and Valentini R 2018 *Proc. Struct. Integ.* **8** 501–8
3. Koyama M, Akiyama E, Lee YK, Raabe D and Tsuzaki K 2017 *Int. J. Hydrog. Energy.* **42** 12706–23
4. Venezuela J, Blanch J, Zulkiply A, Liu Q, Zhou Q, Zhang M and Atrens A 2018 *Corros. Sci.* **135** 120–135
5. Khedr M, Li W, Zhu X, Zhou P, Gao S and Jin X 2018 *Mater. Sci. Eng.* A **712** 133–139
6. Kim HJ, Jeon SH, Yang WS, Yoo BG, Chung YD and Ha HY 2018 *J. Alloy. Compd.* **735** 2067–80

7. Yang J, Song Y, Lu Y, Gu J and Guo Z 2018 *Mater. Sci. Eng.* A **712** 630–636
8. Agyenim-Boateng E, Huang S, Sheng J, Yuan G, Wang Z and Zhou J 2017 *Surf. Coat. Tech.* **328** 44–53
9. Ji H, Park IJ, Lee SM and Lee YK 2014 *J. Alloy. Compd.* **598** 205–212
10. Li X, Wang Y, Zhang P, Li B, Song X and Chen J 2014 *Mater. Sci. Eng.* A **616** 116–122
11. Zhao Y, Lee DH, Kim WJ, Seok MY, Kim JY, Han HN and Suh JY 2018 *Mater. Sci. Eng.* A **718** 43–47
12. Liu J, Guo Q, Yu M and Li S 2014 *Chinese. J. Aeronaut.* **27** 1327–33
13. Wang G, Yan Y, Li J, Huang J, Su Y and Qiao L 2013 *Corros. Sci.* **77** 273–280
14. Azizi S, Salah M, Nefzi H, Khaldi C, Sediri F, Dhahri E and Lamloumi J 2015 *J. Alloy. Compd.* **648** 244–252
15. Nagumo M, Nakamura M and Takai K 2001 *Metall. Mater. Trans.* A **32** 339–347
16. Ronevich JA, De Cooman BC, Speer JG, De Moor E and Matlock DK 2012 *Metall. Mater. Trans.* A **43** 2293–301
17. Takakuwa O, Mano Y and Soyama H 2014 *Int. J. Hydrog. Energy.* **39** 6095–103
18. Daniel P A and Carl J A 1995 *Metall. Mater. Trans.* A **26** 2849–58